RSC Advances

PAPER

View Article Online
View Journal | View Issue

Cite this: *RSC Adv.*, 2021, **11**, 22780

Improvement of low-temperature NH_3-SCR catalytic performance over nitrogen-doped MO_x–Cr_2O_3–La_2O_3/TiO_2–N (M = Cu, Fe, Ce) catalysts†

Xiaoyi Sun, Qingjie Liu, Shuai Liu, Xintang Zhang* and Shanshan Liu*

A series of MO_x–Cr_2O_3–La_2O_3/TiO_2–N (M = Cu, Fe, Ce) catalysts with nitrogen doping were prepared *via* the impregnation method. Comparing the low-temperature NH_3-SCR activity of the catalysts, CeCrLa/Ti–N ($xCeO_2$–yCr_2O_3–zLa_2O_3/TiO_2–N) exhibited the best catalytic performance (NO conversion approaching 100% at 220–460 °C). The physico-chemical properties of the catalysts were characterized by XRD, BET, SEM, XPS, H_2-TPR, NH_3-TPD and *in situ* DRIFTS. From the XRD and SEM results, N doping affects the crystalline growth of anatase TiO_2 and MO_x (M = Cu, Fe, Ce, Cr, La) which were well dispersed over the support. Moreover, the doping of N promotes the increase of the Cr^{6+}/Cr ratio and Ce^{3+}/Ce ratio, and the surface chemical adsorption oxygen content, which suggested the improvement of the redox properties of the catalyst. And the surface acid content of the catalyst increased with the doping of N, which is related to CeCrLa/TiO_2–N having the best catalytic activity at high temperature. Therefore, the CeCrLa/TiO_2–N catalyst exhibited the best NH_3-SCR performance and the redox performance of the catalysts is the main factor affecting their activity. Furthermore, *in situ* DRIFTS analysis indicates that Lewis-acid sites are the main adsorption sites for ammonia onto CeCrLa/TiO_2–N and the catalyst mainly follows the L–H mechanism.

Received 17th May 2021
Accepted 21st June 2021

DOI: 10.1039/d1ra03845a

rsc.li/rsc-advances

1. Introduction

Nitrogen oxides (NO_x) derived from the burning of fossil fuels such as coal and oil are very harmful to human beings and the environment. As one of the main polluting gases, nitrogen oxides not only cause acid rain and photochemical pollution, but also are a major component of PM 2.5.[1] Thus, it is imperative to control the emission of harmful NO_x. In recent years, ammonia selective catalytic reduction (NH_3-SCR) is widely used in the removal of NO_x. In this process, NH_3 is used as a reductant to reduce NO_x in coal-fired flue gas to harmless N_2 and H_2O under the action of a catalyst which is the core of the NH_3-SCR technology. Currently, catalysts with polymetallic oxides as active components are extensively studied.[2–4] The synergistic effect between polymetallic oxides could promote NH_3-SCR performance of the catalysts.

It is well known that ceria is an environmentally-benign material which was widely used as catalysts for NH_3-SCR due to the excellent redox ability of the Ce^{4+}/Ce^{3+} reversible redox pair, rich surface oxygen vacancies and high oxygen storage capacity.[5–7] It has been found that the addition of Ce can increase the high temperature activity of the catalyst.[8,9] Some researchers have reported that Cr-modified Ce–Zr oxide exhibited high NO oxidation activity due to the intense interaction of ad-O_2 and ad-NO accelerated by Cr, which can improve NH_3-SCR performance.[10–12] Furthermore, Lu *et al.*[13] investigated Ce can promote the conversion between Cr^{3+} and Cr^{5+} and increase the proportion of lattice oxygen, which improves the activity of the catalyst. Chromium oxides (CrO_x) have variability of oxidation states, especially for exposed chromium ions, and its most common valence states are Cr^{3+} and Cr^{5+}.[14] CrO_x was found to be one of the most active metals for complete oxidation.[15] Thus, the interaction between Ce and Cr can improve the redox property and accelerate the redox circle, which are beneficial to the improvement of NH_3-SCR activity. Moreover, La is a rare earth element that is abundant in China and since lanthanide oxides possess excellent oxygen storage capacity and unique redox properties, lanthanide-doped catalysts have been widely investigated for SCR reaction.[16,17] La^{3+} could partly incorporate into the ceria fluorite lattice to induce an expansion of the crystal cell dimensions, which concomitantly induces more lattice defects and improves the lattice oxygen mobility.[18] Yi *et al.*[19] studied the effects of rare earth elements (La, Ce) modification on oxidation performance and the results showed that La, Ce modification could promote the oxidation performance of adsorbents, increase the specific surface area, and reduce the pore diameter of the adsorbents. Zhang *et al.*[20] prepared a series of MO_x–V_2O_5–MoO_3–CeO_2/TiO_2 (M = Mn, Cu,

College of Chemical and Biological Engineering, Shandong University of Science and Technology, Qingdao 266590, PR China. E-mail: zhangxt966@126.com; skd996368@sdust.edu.cn

† Electronic supplementary information (ESI) available. See DOI: 10.1039/d1ra03845a

Sb, and La) catalysts to investigate their NH_3-SCR performance, and found that $La_5V_1Mo_3Ce_7$/Ti exhibited the largest number of acid sites, might be suitable for use in high temperature denitrification applications. Therefore, the interaction between Ce and La can improve the redox performance and acidity of the catalyst, which is conducive to the improvement of NH_3-SCR activity.

Copper has been regarded as a prospective active component on account of its low cost, high activity, and green property.[21] As active component, CuO could increase the redox ability in virtue of the poly-valent properties.[22] Donovan *et al.*[23] found that titanium-supported Mn, Cr and Cu performed well at low temperature due to the increase of acid sites on the surface. Liu *et al.*[24] prepared a series of La–Cu–Mn–O catalysts and found that La was conducive to the decrease in the size of Cu and Mn and preventing their agglomeration, enabling the enhancement in reducibility of the catalysts, which promotes the increase in exposed active sites. Furthermore, La^{3+} enhanced the redox couples of $Mn^{4+} + Cu^{+} \leftrightarrow Mn^{3+} + Cu^{2+}$, leading to the formation of high-proportioned active ions (Cu^{2+} and Mn^{3+}) and surface oxygen defects in abundance. Thus, the interaction between Cu and Cr or La is helpful to improve the surface acidity and redox performance of the catalyst, which favours the SCR activity of catalysts. In addition to cerium and copper, iron has been widely used in denitration catalysts because of its environmental friendliness and high activity at medium and high temperature. Ge *et al.*[25] found that the addition of Cr greatly increased the BET surface area, the number of weak and medium–strong acid sites and the ratio of Fe^{3+}/Fe^{2+} on the surface of Fe/AC catalyst, thus promoting the low temperature SCR activity of the catalyst. Hou *et al.*[26] reported that the Brønsted acid sites of Fe–Mn/TiO_2 was significantly improved after La modification. Therefore, the interaction between Fe and Cr or La helps to improve the redox capacity and the number of acid sites on the catalyst.

Furthermore, the supports are also important for the SCR reaction. A good support can disperse the active components well. Moreover, the interaction of supports and active components also has an important effect on the catalytic performance.[27] Currently, anatase TiO_2, Al_2O_3, molecular sieves, and carbon-based materials are usually used as denitrification catalyst supports. Among them, anatase TiO_2 has the advantages of low price, good sulfuric resistance, and non-toxicity.[28] And anatase TiO_2 is favourable to the SCR reaction for the rich Lewis acid sites on the surface.[29] However, anatase TiO_2 often displayed decreasing NH_3-SCR performance due to the crystalline transition of TiO_2 with the temperature increase. In many modified supports,[30–32] it was found that the doped N can inhibit the phase transition of TiO_2 from anatase to rutile. Moreover, the surface acidity, oxygen vacancies, and active sites can also be improved.[33] Devi *et al.* suggested that nitrogen has comparable atomic size with oxygen, small ionization energy, metastable centre formation and stability.[34] Thus, when the N doped TiO_2, the nitrogen can partially substitute oxygen over TiO_2 crystalline. The substitution of nitrogen alters both the electronic properties and surface structure of TiO_2, which the former property determines redox power of carriers, and the latter one control the surface transfer of charge carriers.[35] The improvement of redox property is beneficial to the NH_3-SCR performance improvement. In this paper, the N-doped TiO_2 has been applied to denitrification and the modification indeed improved the NH_3-SCR performance of the CeCrLa/Ti catalysts.

In this paper, MCrLa/TiO_2–N (M = Cu, Fe, Ce), CeCrLa/Ti were prepared *via* an impregnation method. The NH_3-SCR activity of different catalysts was investigated, and a series of characterization techniques (XRD, BET, SEM, XPS, H_2-TPR and NH_3-TPD) were used to explore the influence of the redox performance of TiO_2 modified by N doping on the denitration performance, and compare with the effect of improving the redox performance by modifying the active component. The effect of the addition of N for the surface structure and surface acidity of catalyst were also described. Furthermore, the reasonable reaction mechanism on the CeCrLa/TiO_2–N catalyst was proposed by the *in situ* DRIFTS.

2. Experimental

2.1 Synthesis and characterization of composite materials

2.1.1 Catalyst preparation

Preparation of supports. N-doped TiO_2 preparation, as follows: first, a certain amount of urea (CH_4N_2O, Keshi, China, AR) and metatitanic acid ($TiO(OH)_2$, Xiya Reagent, China, 98%) was dissolved in ethanol (C_2H_5OH, Xilong Scientific, China, AR) by magnetic stirring, the slurry was placed at room temperature for 24 h. Second, the slurry was dried to complete at 100 °C and then calcined at 500 °C for 5 h in air. TiO_2 preparation: $TiO(OH)_2$ was calcined at 500 °C for 3 h in air.

Preparation of catalysts. The catalysts were prepared *via* an impregnation method. Take the preparation of CuCrLa/TiO_2–N catalyst as an example. First, copper nitrate ($Cu(NO_3)_2 \cdot 3H_2O$, Kermel, China, AR), chromium nitrate ($Cr(NO_3)_3 \cdot 9H_2O$, Aladdin, China, AR) and lanthanum nitrate ($La(NO_3)_3 \cdot 6H_2O$, Macklin, China, AR) were dissolved in ethanol, the solution was stirred until all solids are dissolved, then the solution was added to the N-doped TiO_2 carrier to ensure that they are evenly mixed. Second, the slurry was placed at room temperature for 24 h. Third, the slurry was dried to complete at 100 °C and then calcined at 500 °C for 5 h in air. The preparation of other catalysts is similar to CuCrLa/TiO_2–N, the difference is the change of active component ($Cu(NO_3)_2 \cdot 3H_2O$ was changed to ferric nitrate ($Fe(NO_3)_3 \cdot 9H_2O$, SCR, China, AR), cerium nitrate ($Ce(NO_3)_3 \cdot 6H_2O$, Macklin, China, AR)) and carrier (N-doped TiO_2 was converted to $TiO(OH)_2$, TiO_2).

2.1.2 Catalyst characterization

X-ray diffraction (XRD). An X-ray diffractometer (Rigaku Ultima IV) was used in determining the catalyst crystal structures using these parameters: scanning at 2θ range from 10° to 80°, radiation at 40 mA and 40 kV with Cu Kα ($\lambda = 0.15406$ nm).

Brunauer–Emmett–Teller surface area analysis (BET). Micromeritics ASAP 2460 was used to perform the test of N_2 adsorption–desorption for the measurement of the textural characteristics of the catalysts at liquid nitrogen temperature −196 °C. To remove physically adsorbed species, the catalysts were pre-degassed for 10 h at 200 °C before each analysis. The

pore size distribution and specific surface area of the catalysts were calculated using the Barrett–Joyner–Halenda (BJH) method and the Brunauer–Emmett–Teller (BET) equation.

Scanning electron microscopy (SEM). FEI Apreo was used to examine the morphology of the catalysts. The sample was dispersed on the conductive adhesive, and then sprayed gold to observe.

X-ray photoelectron spectroscopy (XPS). Escalab 250Xi with a monochromatic Al-Kα target ($h\nu$ = 1486.6 eV) was used to obtain X-ray photoelectron spectroscopy (XPS) of the samples. Before the test, the samples were outgassed in a UHV chamber ($<10^{-7}$ Pa). The calibration of binding energies of N 1s, O 1s, Ti 2p, Cr 2p, Ce 3d was obtained by using C 1s peak (284.8 eV). Peak fitting is done using XPSPEAK 4.1 with a Shirley background.

Hydrogen temperature programmed reduction (H_2-TPR). A chemisorption apparatus (Micromeritics ChemiSorb 2720) with 0.2 g catalyst was used to collect H_2-TPR profiles. Before that, the samples were pretreated in pure Ar atmosphere for 1 h at 300 °C and then cooled down to 50 °C for half an hour to mix the gas 10% H_2/Ar. The TPR profiles of the catalysts were collected when the baseline remained unchanged by heating the samples from 50 to 800 °C at a rate of 10 °C min^{-1}, with aggregation rate of 25 mL min^{-1} with 10% H_2/Ar. Thermal conductivity detectors were taken in continuously monitoring H_2 consumption.

Ammonia temperature programmed desorption (NH_3-TPD). A chemisorption apparatus (Micromeritics Auto Chem II 2920) with 0.2 g catalyst was used to collect NH_3-TPD profiles. Before that, the catalysts were preheated for 1 h at 300 °C in a helium flow and then cooled down to 100 °C for 5% NH_3/He 1 h. The physically adsorbed NH_3 was removed by purging He for another 1 h. When the samples were heated at a rate of 10°C min^{-1} from 100 to 500 °C, with aggregation rate of 50 mL min^{-1} with He, the profiles of the catalysts were recorded.

In situ diffuse reflectance infrared Fourier transform spectroscopy (in situ DRIFTS). A Bruker VERTEX 70 spectrometer with a highly sensitive MCT detector set to a resolution of 4 cm^{-1} with a scan count of 64 was used to carry out *in situ* DRIFTS experiments. And the samples were prepared by the KBr tableting method.

2.2 Catalytic performance measurement

In this work, a fixed-bed flow reactor containing 3 mL catalyst of 40–60 mesh was taken for testing SCR activities. The reaction condition was controlled as follows: 1000 ppm NO, 1000 ppm NH_3, 5% O_2, and the balance gas is N_2. The gas hourly space velocity (GHSV) was approximately 20 000 h^{-1}, with a sum rate of 1000 mL min^{-1} of the feed gas. The NO concentration was measured with a signal NO_x analyser (KM945, KANE, UK), reaction temperatures were recorded at an interval of at least 30 min in each test. The following equation was used to calculate NO conversion:

$$\text{NO conversion } (\%) = \frac{[\text{NO}]_{\text{in}} - [\text{NO}]_{\text{out}}}{[\text{NO}]_{\text{in}}} \times 100\% \quad (1)$$

3. Results and discussion

3.1 Catalytic properties of composite materials

NH_3-SCR performance of CuCrLa/TiO_2–N, FeCrLa/TiO_2–N, CeCrLa/TiO_2–N, CeCrLa/$TiO(OH)_2$ and CeCrLa/TiO_2 catalysts were evaluated as a function of temperature, and the results are illustrated in Fig. 1. From Fig. 1, compared with CuCrLa/TiO_2–N and FeCrLa/TiO_2–N, NO conversion of CeCrLa/TiO_2–N increased with temperature from 140 °C to 300 °C, and it was stable at over 96% between 220–460 °C, which indicates that the synergistic effect of Ce, Cr, La plays a more important role in improving the catalytic activity, or CeCrLa/TiO_2–N has the best synergistic effect between oxidation reducibility and acidity. Furthermore, CeCrLa/TiO_2–N showed higher activity than CeCrLa/$TiO(OH)_2$ and CeCrLa/TiO_2 in the whole temperature range, which might be due to the addition of N promoting the redox performance, especially at low temperatures (<340 °C). Moreover, NO conversion of the CeCrLa/TiO_2–N catalyst was stable at over 96% between 220–460 °C, compared with catalysts prepared in other studies,[8,15,20] the temperature window is wider and the low-temperature performance is better.

3.2 Structural characterizations of catalysts

The XRD patterns of the catalysts are shown in Fig. 2. As seen, all samples display diffraction peaks at 25.3°, 37.8°, 48.1°, 53.9°, 55.1°, 62.8°, 68.7°, 70.4° and 75.1°, which correspond to anatase TiO_2 phase peaks [PDF-JCPDS 21-1272]. No independent diffraction peaks related to CuO_x, FeO_x, CeO_x, CrO_x and LaO_x were observed in all samples. This indicates that the supported metal oxides were in a highly dispersed state. The good dispersion facilitated good contact of the active components with each other, and led to strong interactions between Ti and other metal oxides.[36] Moreover, good dispersion can increase the effective area, which improves the activity of the catalyst. According to the Debye–Scherrer's formula, the crystalline size was calculated and listed in Table 1. The crystal size increased in the following sequence: CeCrLa/$TiO(OH)_2$ < CeCrLa/TiO_2 < CeCrLa/TiO_2–N < FeCrLa/TiO_2–N < CuCrLa/TiO_2–N. The different crystal size shows that N doping promotes the crystalline growth of anatase TiO_2,[37] Fe, Cu and Ti oxide had interaction, and that the crystallite size increased in different extent.

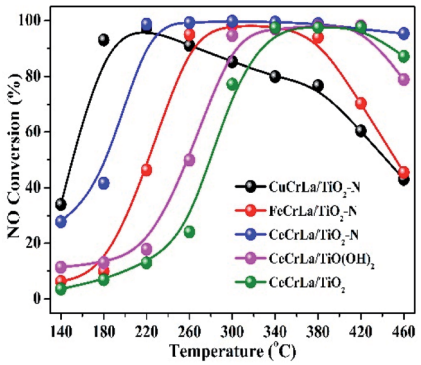

Fig. 1 NO conversion of the catalysts. Reaction conditions: [NO] = [NH_3] = 1000 ppm, [O_2] = 5%, N_2 balance, GHSV = 20 000 h^{-1}.

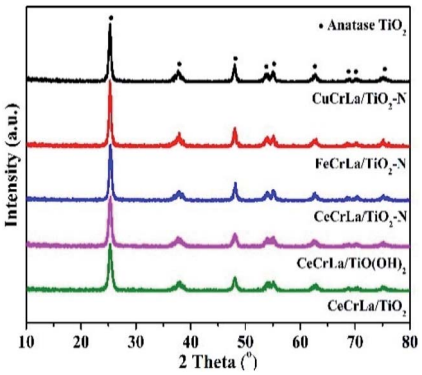

Fig. 2 XRD patterns of all samples.

The N_2 adsorption–desorption isotherms of the catalysts are presented in Fig. S1.† The BET surface areas, total pore volumes and average pore diameters of all samples are summarized in Table 1. As shown in Fig. S1(a),† the samples showed isotherms of type III, which exhibited hysteresis loops mostly of type H3, indicating that these samples contained mesopores (2–50 nm). Larger surface area and smaller average pore size contribute to the higher physisorption ability of catalyst. $CeCrLa/TiO(OH)_2$ and $CeCrLa/TiO_2$ with the stronger physical adsorption capacity compared with MCrLa/Ti–N (M = Cu, Fe, Ce) catalysts has the lower catalytic activity at low temperature, indicating that the addition of N has little effect on the BET surface area and pore size distribution. Based on these results, it appears that the textural parameters did not play an important role in this catalytic reaction system.

SEM test was carried out to observe the morphology of all samples. It can be observed in Fig. 3 that there is no significant difference in the morphology of the five catalysts. The catalysts are in the form of particles and they have aggregated.

3.3 XPS analysis

To characterize the elemental state at the surface of the catalysts, a series of XPS studies were carried out in this paper, as shown in Fig. 4, and the surface element concentrations were listed in Table 2.

The N 1s spectra as shown in Fig. 4(a) was deconvoluted into two component peaks located in the range of 397.8–398.1 eV and 400.6–400.9 eV. The characteristic peak at around 397.9 eV is attributed to O–Ti–N structures generated upon the replacement of O atoms in the TiO_2 network.[38] Furthermore, the peak

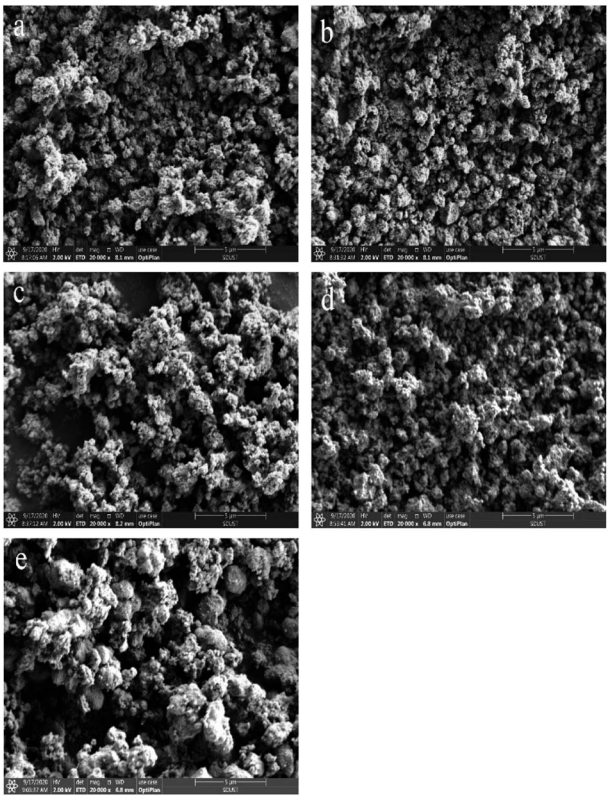

Fig. 3 SEM images obtained for: (a) $CuCrLa/TiO_2$–N, (b) $FeCrLa/TiO_2$–N, (c) $CeCrLa/TiO_2$–N, (d) $CeCrLa/TiO(OH)_2$, (e) $CeCrLa/TiO_2$.

at 400.8 eV can be assigned to O–Ti–O–N bonds, indicating that N atoms doped in the TiO_2 lattice in the interstitial sites.[39] From the XPS results, the existence of compounds O–Ti–N and O–Ti–O–N confirms that nitrogen atoms have been doped into the lattice of TiO_2. It was reported that the nitrogen atoms replaced the oxygen atoms in the lattice of TiO_2; which led to the production of a large number of oxygen vacancies.[40] And the substitution of nitrogen alters the electronic properties of TiO_2, which can improve the redox power of carriers.[34] This is in agreement with $CeCrLa/TiO_2$–N exhibiting the best NH_3-SCR performance among the CeCrLa/Ti catalysts.

The O 1s XPS spectra of all catalysts are shown in Fig. 4(b). Based on the results reported in previous studies,[41,42] the O 1s XPS spectra could be spilt into two peaks: lattice oxygen (B.E. = 530.0–530.4 eV, denoted as O_β), chemisorbed oxygen (B.E. = 531.6–532.2 eV, denoted as O_α). The content of surface adsorbed

Table 1 XRD and BET results of all the samples

Samples	Crystal size (nm)	BET surface area ($m^2\ g^{-1}$)	Pore volume ($cm^3\ g^{-1}$)	Average pore diameter (nm)
$CuCrLa/TiO_2$–N	19	74	0.21	14
$FeCrLa/TiO_2$–N	18	78	0.22	14
$CeCrLa/TiO_2$–N	15	80	0.21	14
$CeCrLa/TiO(OH)_2$	13	90	0.24	14
$CeCrLa/TiO_2$	14	82	0.20	9

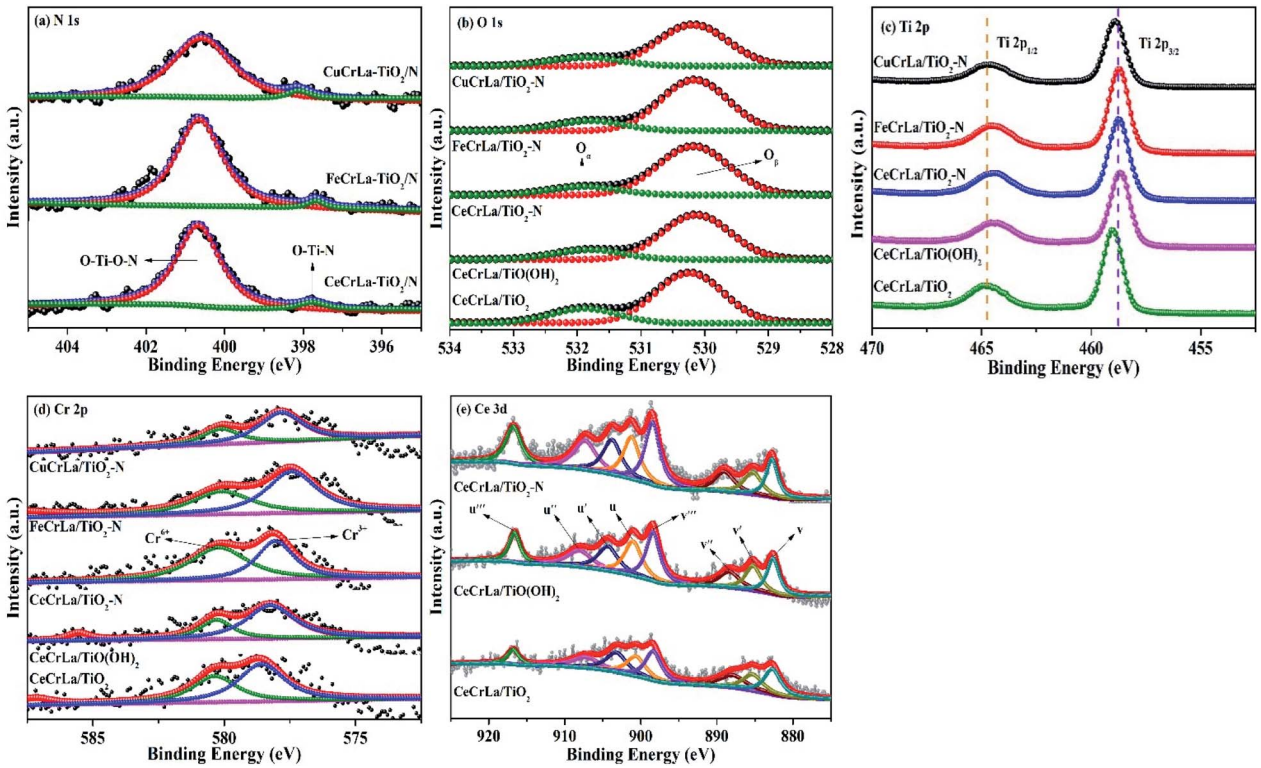

Fig. 4 (a) N 1s, (b) O 1s, (c) Ti 2p, (d) Cr 2p XPS spectra of all samples, (e) Ce 3d XPS spectra of the CeCrLa/Ti catalysts.

oxygen over these catalysts is calculated as $O_\alpha/(O_\alpha + O_\beta)$ and listed in Table 2. The mobility of the surface chemisorbed oxygen is stronger than the lattice oxygen, thus it is easier to participate in the NH_3-SCR reaction.[43–45] In general, the high $O_\alpha/(O_\alpha + O_\beta)$ relative concentration ratio on the catalyst surface could be related to high SCR activity.[46] It could be distinctly seen in Table 2 that the ratio of O_α on the CeCrLa/Ti catalysts were higher than that on CuCrLa/TiO_2–N and FeCrLa/TiO_2–N, indicating that Ce is more conducive to the production of chemisorbed oxygen adsorption site on the catalyst surface. Moreover, the ratio of O_α on CeCrLa/$TiO(OH)_2$ and CeCrLa/TiO_2 were higher than that on CeCrLa/TiO_2–N, this might be because N replaced the adsorbed oxygen or N inhibited the oxygen mobility,[47] and this indicate that moderate surface chemisorbed oxygen content is more conducive to high SCR activity and chemisorbed oxygen may not play an important role in this catalytic reaction system.

The XPS of Ti 2p can be fitted into two peaks. The peaks located at around 458.9 and 464.7 eV could be the result of the orbitals of Ti $2p_{1/2}$ and Ti $2p_{3/2}$, respectively. This indicated that Ti existed in Ti^{4+} oxidation state.[48,49] It is observed that the binding energy of MCrLa/TiO_2–N (M = Cu, Fe, Ce) shift to lower values compared with that of CeCrLa/TiO_2, which means that Ti^{4+} partially reduces to Ti^{3+} due to the nitrogen species in TiO_2 changing the electron density distribution of Ti atoms.[50] That will increase the amount of defective active site and will be more beneficial to the adsorption of NH_3 and NO_x species, thereby promoting to the SCR reaction.[36]

Table 2 Redox properties measured for the different catalysts from H_2-TPR data and the surface compositions of the samples derived from XPS data

Samples	H_2 consumption[a] (10^{-5} mmol g^{-1})					Total H_2 consumption[b] (10^{-5} mmol g^{-1})	Surface atomic content[c] (%)					Percent of valence state[d] (%)			
	Peak 1	Peak 2	Peak 3	Peak 4	Peak 5		Ce	Cr	Ti	O	N	N_s/N^e	Ce^{3+}/Ce	Cr^{6+}/Cr	O_α/O
CuCrLa/TiO_2–N	10.2	7.5	8.6	1.4	1.0	28.7	—	0.8	36.5	59.0	2.5	4.3	—	12.2	9.0
FeCrLa/TiO_2–N	3.3	3.7	11.8	2.6	3.8	25.2	—	0.7	37.8	58.2	2.9	2.8	—	30.6	10.6
CeCrLa/TiO_2–N	4.2	5.4	12.1	5.8	3.6	31.1	0.1	0.8	37.8	58.4	2.8	4.6	22.1	35.4	11.1
CeCrLa/$TiO(OH)_2$	2.3	3.2	9.0	10.4	—	24.9	0.1	0.7	39.1	60.1	—	—	18.7	13.6	13.0
CeCrLa/TiO_2	2.5	3.3	7.6	9.8	—	23.2	0.1	0.7	36.6	62.4	—	—	15.5	25.2	18.0

[a] The H_2 consumption over catalysts. [b] The total H_2 consumption over catalysts. [c] The content of various elements determined by XPS. [d] The percent of valence state on the surface of catalysts. [e] The substituted N.

The XPS spectra for Cr 2p of all samples are given in Fig. 4(d) and show that two distinct peaks corresponding to Cr^{3+} (577.6–578.8 eV), and Cr^{6+} (579.8–581.0 eV).[10,14] It has been reported that Cr addition could facilitate the SCR performance by the valence change between Cr^{6+} and lower oxidized states (Cr^{5+}, Cr^{3+} and Cr^{2+}).[51] From Fig. 5(d), it was obvious that the binding energy of Cr in CeCrLa/Ti catalysts shifted to the high field compared with CuCrLa/TiO_2–N and FeCrLa/TiO_2–N, indicating that the Cr undergone oxidation reaction, and the binding energy was shifted toward the high energy direction. The addition of Ce promotes the conversion between Cr^{3+} and Cr^{6+}, improving the redox performance of the catalyst.[11] As seen in Table 2, the ratio of Cr^{6+}/Cr on CeCrLa/TiO_2–N is the largest, which corresponds to the high NH_3-SCR activity of CeCrLa/TiO_2–N.

The Ce 3d XPS spectra of CeCrLa/Ti catalysts are presented in Fig. 4(e). According to previous studies,[5,49,52] the Ce 3d XPS spectra could be separated into 8 peaks and "u" and "v" were attributed to Ce $3d_{3/2}$ and Ce $3d_{5/2}$, respectively. The two peaks labelled u′ and v′ could be assigned to Ce^{3+}, with the remaining peaks of u, u″, u‴, v, v″ and v‴ belonging to Ce^{4+}.[53,54] The ratio of Ce^{3+}/Ce for the CeCrLa/Ti samples could be calculated from the results of XPS analysis and the results are listed in Table 2. Obviously, the ratio of Ce^{3+}/Ce over CeCrLa/TiO_2–N is higher than that of CeCrLa/$TiO(OH)_2$ and CeCrLa/TiO_2. This indicates that the introduction of N has promoted the conversion of Ce^{4+} to Ce^{3+}. It can be speculated that N can provide electrons to promote the conversion of Ce^{4+} to Ce^{3+}, which directly leads to the highest Ce^{3+}/Ce ratio of CeCrLa/TiO_2–N among the CeCrLa/Ti catalysts.

3.4 H_2-TPR analysis

The redox property of the samples was determined by H_2-TPR analysis, and the results are shown in Fig. 5. It is apparent that there is one reduction peak in the profile of N-doped TiO_2, and it could be attributed to $Ti^{4+} \rightarrow Ti^{3+}$.[55] From Fig. 5(a), there are five peaks appear from 200 to 700 °C in the H_2-TPR profile of MCrLa/TiO_2–N (M = Cu, Fe, Ce). It has been reported that CuO_x species have a great degree of reduction capacity at lower temperatures.[56] Thus, the first peak of CuCrLa/TiO_2–N appeared at 244 °C can be assigned to $Cu^{2+} \rightarrow Cu^{+}$, which is lower than that of FeCrLa/TiO_2–N and CeCrLa/TiO_2–N and as for the excellent redox property at lower temperatures, CuCrLa/TiO_2–N displayed the best low-temperature performance (NO conversion >90% at 180–220 °C). Furthermore, the reduction peak temperature sequence of the samples is consistent with the order of their low-temperature (<220 °C) activity, which is CuCrLa/TiO_2–N > CeCrLa/TiO_2–N > FeCrLa/TiO_2–N > CeCrLa/$TiO(OH)_2$ > CeCrLa/TiO_2. As listed in Table 2, total H_2 consumption of CeCrLa/TiO_2–N was the highest among MCrLa/TiO_2–N (M = Cu, Fe, Ce), which indicates that the synergistic effect between Ce, Cr and La was more conducive to promoting the high-temperature SCR activity.

For CeCrLa/$TiO(OH)_2$ and CeCrLa/TiO_2, four obvious reduction peaks can be seen, and the first peaks could be attributed to $Cr^{6+} \rightarrow Cr^{3+}$, the second peaks might be assigned as $Cr^{3+} \rightarrow Cr^{0}$, the third peaks might due to $Ce^{4+} \rightarrow Ce^{3+}$, the fourth peaks could be considered as co-reduction of $Ce^{3+} \rightarrow Ce^{0}$ and $Ti^{4+} \rightarrow Ti^{3+}$. It can be clearly seen from Fig. 5(b) that the reduction peaks of CeCrLa/TiO_2–N moves toward lower temperatures compared with CeCrLa/$TiO(OH)_2$ and CeCrLa/TiO_2, suggesting that the reducibility increased with the changes in the surface chemical environment after N-doping. As listed in Table 2, the reducibility among catalysts doped with N enhanced at low temperatures, thus MCrLa/TiO_2–N (M = Cu, Fe, Ce) exhibited higher NO conversion at low temperatures.

3.5 NH_3-TPD analysis

NH_3-TPD tests were performed and the results are shown in Fig. 6. From Fig. 6, three peaks appear from 100 to 500 °C in the NH_3-TPD profile of each catalyst. The peaks at the range of 150–200 °C, 250–370 °C and 400–500 °C refer to weak acid, medium-strength acid, and high-strength acid, respectively.[57–59] According to literature,[60] the medium-strength and high-strength acid sites are effective for NO reduction at moderate to high temperature. As seen from Fig. 6, compared with CuCrLa/TiO_2–N and FeCrLa/TiO_2–N, the desorption peaks of CeCrLa/TiO_2–N shifts to a higher temperature range, suggesting that the strength of the acid sites on CeCrLa/TiO_2–N is stronger. Furthermore, the peak area of CeCrLa/TiO_2–N increased with the introduction of N by comparing the NH_3-TPD results of the CeCrLa/Ti samples. This indicates that the doping of nitrogen promotes the increase of

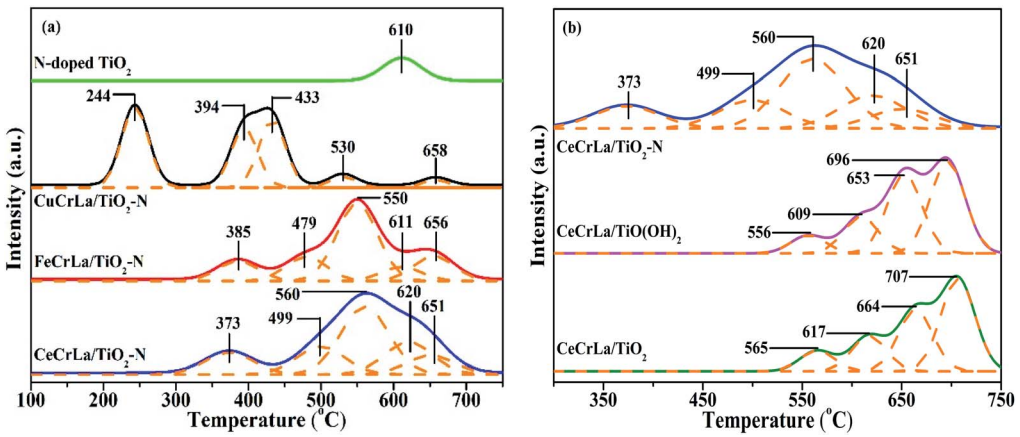

Fig. 5 H_2-TPR profiles of (a) MCrLa/TiO_2–N and (b) CeCrLa/Ti catalysts.

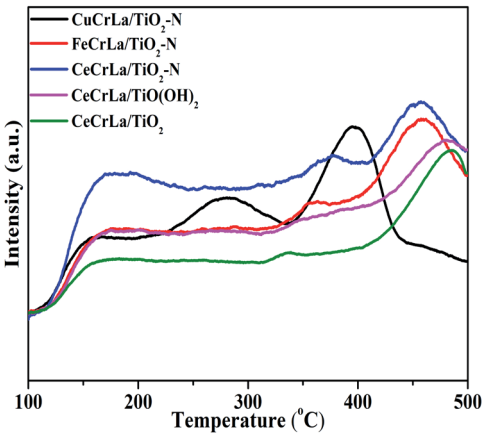

Fig. 6 NH_3-TPD profiles of all samples.

acid sites on the surface of CeCrLa/TiO_2–N. The CeCrLa/TiO_2–N presents the largest NH_3 adsorption capacity, which is helpful to promote the NH_3-SCR reaction over it. However, it can be clearly seen that the peak area of medium-strength acid of CuCrLa/TiO_2–N is the widest, which does not conform to its activity. It might be related to the formation of copper ammonium complex ions.[61]

3.6 Investigation of reaction mechanism

In order to explore the activation ability of the catalyst, the formation and transformation of surface species, the sample with the best catalytic activity, CeCrLa/TiO_2–N, was selected for *in situ* DRIFTS characterization (NH_3 pre-adsorption and then NO + O_2, NO + O_2 pre-adsorption and then NH_3).

3.6.1 NH_3 pre-adsorption and then NO + O_2. In order to compare the reactivity of the adsorbed NH_3 species in the SCR reaction, *in situ* DRIFTS spectra of the reaction between NO + O_2 and pre-adsorbed NH_3 was recorded. As shown in Fig. 7(a), after the adsorption of 1000 ppm NH_3 for 30 min at 200 °C, CeCrLa/TiO_2–N was covered by coordinated NH_3 species bound to Lewis-acid sites (1224, 1282 and 1649 cm^{-1}), NH_2 species (1334, 1533 and 1566 cm^{-1}).[8,62,63] After injecting NO + O_2 for 10 min, all the bands belonging to ammonia adsorption species disappeared, accompanied by the bands corresponding to NO_x species. The surface of the catalyst was covered by bridging nitrites (1206 cm^{-1}), monodentate nitrates (1263 cm^{-1}), bidentate nitrates (1302 and 1548 cm^{-1}), M–NO_2 nitro compounds (1345 and 1425 cm^{-1}), and bridging nitrates (1612 cm^{-1}).[10,64] And the band at 3653 cm^{-1} could be attributed to the free –OH stretching vibration.[37]

3.6.2 NO + O_2 pre-adsorption and then NH_3. Fig. 7(b) shows the spectra of the reaction between NH_3 and pre-adsorbed NO + O_2 over the CeCrLa/TiO_2–N catalyst at 200 °C. As shown in illustration, after the adsorption of 1000 ppm NO and 5% O_2 for 30 min at 200 °C, CeCrLa/TiO_2–N was covered by bridging nitrates (1241 and 1612 cm^{-1}), M–NO_2 nitro compounds (1327 and 1356 cm^{-1}), monodentate nitrates (1381 cm^{-1}), bidentate nitrates (1548 cm^{-1}).[53,64] Several bands appeared after the introduction of NH_3, it took about 1 min to consume all ad-NO_x. After 30 min, the surface of the catalyst was covered by coordinated NH_3 bound to Lewis-acid sites (1263, 1289 and 1634 cm^{-1}), NH_2 species (1339 cm^{-1}), monodentate nitrites (1430 and 1471 cm^{-1}), bridging nitrates (1570 and 1601 cm^{-1}), NH_4^+ species on Brønsted-acid sites (1692 cm^{-1}), N–H stretching mode of adsorbed NH_3 (3157, 3252 and 3336 cm^{-1}).[41,53,62] Additional band at 3658 cm^{-1} was a characteristics band for the hydroxyl group.[37]

3.6.3 Mechanism analysis. When NH_3 passes over pre-adsorbed NO + O_2 on the catalyst, all of the NO_x related bands quickly disappeared in less than 1 min, while NO + O_2 passing over pre-adsorbed the NH_3, it took about 10 min to consume all the NH_3 associated bands. This indicate that the catalyst is more likely to adsorb NH_3, which means that the surface of the catalyst has much acid sites, and this is conducive to the improvement of NH_3-SCR activity of the catalyst. According to the report[65] that Lewis-acid sites were the main active sites for NH_3 activation at low temperatures (<250 °C). As shown in Fig. 7(a), after NH_3 adsorption, all the ammonia adsorption species on CeCrLa/TiO_2–N belonging to Lewis-acid sites, which confirmed that Lewis-acid sites are the main adsorption sites for ammonia onto the CeCrLa/TiO_2–N catalyst. While for the NH_2 species can react with gaseous NO or NO_2 to form NH_2NO or NH_2NO_2 species,[66] which further dissociate into N_2 and H_2O (E–R mechanism). However, neither NH_2NO_x species nor gaseous NO, NO_2 were observed, which is possibly because they are transformed and consumed quickly. Therefore, it was proposed that the reaction mainly occurs between the adsorbed NH_3 and the adsorbed nitrates, following the L–H mechanism.[10] Combined with XPS analysis, the changing of metal ion valence state would promote the generation of oxygen vacancy on the surface of catalytic, which was mainly responsible for NO adsorption and nitrate formation.[66] Thus, according to Fig. 7(a and b), the SCR reaction on CeCrLa/TiO_2–N could be facilitated through the following pathway (□ denotes an oxygen vacancy):[10,65–67]

$$NH_3(g) \xrightarrow{Ce^{4+}/Cr^{6+}} NH_3(a) \rightarrow -NH_2 \overset{-H}{\rightarrow} -NH \quad (2)$$

$$NH_3(g) \xrightarrow{Ce^{3+}/Cr^{3+}} NH_4^+(a) \quad (3)$$

$$NO(g) \xrightarrow{Ce^{4+}/Cr^{6+}} NO(a) \quad (4)$$

$$O_2(g) + \square \rightarrow 2O(a) \quad (5)$$

$$NO(a) + O(a) \rightarrow \text{monodentate, bidentate, and bridging nitrates, monodentate nitrites} \quad (6)$$

$$NH_3(a)/-NH_2/NH_4^+(a) + \text{monodentate/bidentate/bridging nitrates, monodentate nitrites} \rightarrow N_2 + H_2O \quad (7)$$

4. Conclusions

In the present work, a series of MCrLa/Ti–N (M = Cu, Fe, Ce) and CeCrLa/Ti catalysts were prepared. The main purpose was to investigate how the physico-chemical properties and

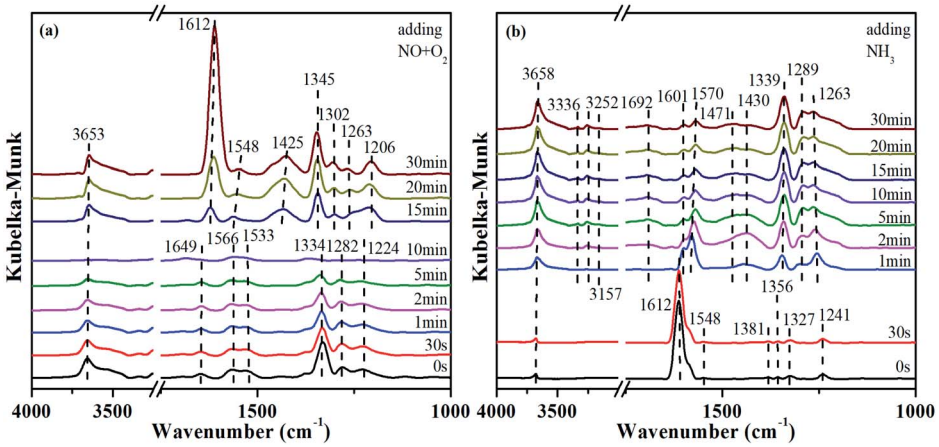

Fig. 7 (a) *In situ* DRIFTS spectra of reaction between (a) NO + O_2 and pre-adsorbed NH_3, (b) NH_3 and pre-adsorbed NO + O_2 over the CeCrLa/TiO_2–N catalyst at 200 °C.

NH_3-SCR performance of the catalysts was influenced as a function of the support modified by N. Some interesting conclusions can be drawn from the characterization results as follows: N doping affects the crystalline growth of anatase TiO_2. Moreover, the doping of N promotes the increase of Cr^{6+}/Cr ratio, Ce^{3+}/Ce ratio, and the surface chemical adsorption oxygen content, which is reflected in the improvement of the oxidation-reduction capacity. And the surface acid content of the catalyst increased with the doping of N, which related to the best catalytic activity of CeCrLa/TiO_2–N at high temperature. Therefore, CeCrLa/TiO_2–N exhibited the highest catalytic activity among these catalysts. From the above discussion, the conclusion can be reached that the N-doped TiO_2 as catalyst support is indeed beneficial to the improvement of NH_3-SCR performance of catalysts. And *in situ* DRIFTS analysis indicates that the reaction between NH_3 adsorption species and ad-NO_x species mainly occurred on the catalyst followed L–H mechanism.

Author contributions

Xiaoyi Sun: writing-original draft, data curation, investigation, formal analysis. Qingjie Liu: investigation. Shuai Liu: validation. Xintang Zhang: conceptualization, resources, supervision. Shanshan Liu: writing-review & editing, formal analysis, project administration.

Conflicts of interest

There are no conflicts to declare.

Acknowledgements

Thanks are due to Professor Zhang for advice on experimental design. I wish to thank the timely help from Dr Liu in analyzing the large number of samples and the article writing. Additional thanks are due to Qingjie Liu and Shuai Liu for help on experimental operation. This research did not receive any specific grant from funding agencies in the public, commercial, or not-for-profit sectors.

References

1 S. Ren, F. Q. Guo, J. Yang, L. Yao, Q. Zhao and M. Kong, *Chem. Eng. Res. Des.*, 2017, **126**, 278–285.
2 B. Thirupathi and P. G. Smirniotis, *Appl. Catal., B*, 2011, **110**, 195–206.
3 M. Saeidi and M. Hamidzadeh, *Res. Chem. Intermed.*, 2016, **43**, 2143–2157.
4 L. L. Guo, L. Liu, X. L. Zhu, Q. Zhang and C. Y. Li, *J. Fuel Chem. Technol.*, 2017, **45**, 723–730.
5 L. Chen, Q. L. Wang, X. X. Wang, Q. L. Cong, H. Y. Ma, T. J. Guo, S. J. Li and W. Li, *Chem. Eng. J.*, 2020, **390**, 124251.
6 C. Liu, L. Chen, J. Li, L. Ma, H. Arandiyan, Y. Du, J. Xu and J. Hao, *Environ. Sci. Technol.*, 2012, **46**, 6182–6189.
7 R. H. Gao, D. S. Zhang, P. Maitarad, L. Y. Shi, T. Rungrotmongkol, H. R. Li, J. P. Zhang and W. G. Cao, *J. Phys. Chem. C*, 2013, **117**, 10502–10511.
8 P. Sun, R. T. Guo, S. M. Liu, S. X. Wang, W. G. Pan, M. Y. Li, S. W. Liu, J. Liu and X. Sun, *Mol. Catal.*, 2017, **433**, 224–234.
9 L. Chen, J. H. Li, M. F. Ge, L. Ma and H. Z. Chang, *Chin. J. Catal.*, 2011, **32**, 836–841.
10 Z. Y. Wang, R. T. Guo, Z. Z. Guan, X. Shi, W. G. Pan, Z. G. Fu, H. Qin and X. Y. Liu, *Appl. Surf. Sci.*, 2019, **485**, 133–140.
11 W. Cai, Q. Zhong, S. L. Zhang and J. X. Zhang, *RSC Adv.*, 2013, **3**, 7009–7015.
12 W. Cai, Q. Zhong, Y. Yu and S. Dai, *Chem. Eng. J.*, 2016, **288**, 238–245.
13 M. Lu, H. L. Hou, C. Y. Wei, X. H. Guan, W. Wei and G. S. Wang, *Catalysts*, 2020, **10**, 140.
14 J. Su, W. Y. Yao, Y. Liu and Z. B. Wu, *Appl. Surf. Sci.*, 2017, **396**, 1026–1033.
15 J. X. Zhang, S. L. Zhang, W. Cai and Q. Zhong, *Appl. Surf. Sci.*, 2013, **268**, 535–540.
16 F. Bin, X. L. Wei, B. Li and K. S. Hui, *Appl. Catal., B*, 2015, **162**, 282–288.

17 Q. Gao, S. Han, Q. Ye, S. Y. Cheng, T. F. Kang and H. X. Dai, *Catalysts*, 2020, **10**, 336.
18 P. Lu, C. T. Li, G. M. Zeng, L. J. He, D. L. Peng, H. F. Cui, S. H. Li and Y. B. Zhai, *Appl. Catal., B*, 2010, **96**, 157–161.
19 H. H. Yi, K. Yang, X. L. Tang, S. Z. Zhao, F. Y. Gao, Y. H. Huang, Y. R. Shi, X. Z. Xie and R. C. Zhang, *Ind. Eng. Chem. Res.*, 2019, **58**, 5423–5431.
20 D. J. Zhang, Z. R. Ma, B. D. Wang, Q. Sun, W. Q. Xu and T. Zhu, *J. Rare Earths*, 2020, **38**, 157–166.
21 Z. C. Si, D. Weng, X. D. Wu, J. Li and G. Li, *J. Catal.*, 2010, **271**, 43–51.
22 C. M. Chen, Y. Cao, S. T. Liu, J. M. Chen and W. B. Jia, *Appl. Surf. Sci.*, 2019, **480**, 537–547.
23 A. P. Donovan, S. U. Balu and G. S. Panagiotis, *J. Catal.*, 2004, **221**(2), 421–431.
24 T. K. Liu, L. Q. Wei, Y. Y. Yao, L. H. Dong and B. Li, *Appl. Surf. Sci.*, 2021, **546**, 148971.
25 T. T. Ge, B. Z. Zhu, Y. L. Sun, W. Y. Song, Q. L. Fang and Y. X. Zhong, *Environ. Sci. Pollut. Res. Int.*, 2019, **26**, 33067–33075.
26 X. X. Hou, H. P. Chen, Y. H. Liang, Y. L. Wei and Z. Q. Li, *Catal. Surv. Asia*, 2020, 291–299.
27 J. B. Tong, Y. Lin, S. L. Liu, J. T. Wen and Y. Y. Liu, *Chem. Ind. Eng. Prog.*, 2014, **33**, 1170–1179.
28 X. Y. Liu, P. Zhang, Y. Y. Jia, Z. H. Tang, G. L. Liu and S. F. Wu, *Environ. Prot. Chem. Ind.*, 2020, **40**, 26–31.
29 Y. Ganjkhanlou, T. V. W. Janssens, P. N. R. Vennestrøm, L. Mino, M. C. Paganini, M. Signorile, S. Bordiga and G. Berlier, *Appl. Catal., B*, 2020, **278**, 119337.
30 N. Kaur, S. K. Shahi, J. S. Shahi, S. Sandhu, R. Sharma and V. Singh, *Vacuum*, 2020, **178**, 109429.
31 S. M. Reda, M. Khairy and M. A. Mousa, *Arabian J. Chem.*, 2020, **13**, 86–95.
32 W. J. Bao, H. X. Chen, H. Wang, R. D. Zhang, Y. Wei and L. R. Zheng, *ACS Appl. Nano Mater.*, 2020, **3**, 2614–2624.
33 C. M. Chen, Y. Cao, S. T. Liu, J. M. Chen and W. B. Jia, *Chin. J. Catal.*, 2018, **39**, 1347–1365.
34 L. G. Devi and R. Kavitha, *Appl. Catal., B*, 2013, **140**, 559–587.
35 F. Veisi, M. A. Zazouli, J. Y. Charati, M. A. Ebrahimzadeh and A. S. Dezfoli, *Environ. Sci. Pollut. Res.*, 2016, **23**, 21846–21860.
36 S. Z. Xie, L. L. Li, L. J. Jin, Y. H. Wu, H. Liu, Q. J. Qin, X. L. Wei, J. X. Liu, L. H. Dong and B. Li, *Appl. Surf. Sci.*, 2020, **515**, 146014.
37 P. S. Jadhav, T. Jadhav, M. Bhosale, C. H. Jadhav and V. C. Pawar, *Mater. Today: Proc.*, 2020, **43**, 2763–2767.
38 S. P. Kunde, K. G. Kanade, B. K. Karale, H. N. Akolkar, S. S. Arbuj, P. V. Randhavane, S. T. Shinde, M. H. Shaikh and A. K. Kulkarni, *RSC Adv.*, 2020, **10**, 26997–27005.
39 C. Zhao, Z. H. Wang, X. Chen, H. Y. Chu, H. F. Fu and C. C. Wang, *Chin. J. Catal.*, 2020, **41**, 1186–1197.
40 K. Choi, J. Bang, I. Moon, K. Kim and J. Oh, *J. Alloys Compd.*, 2020, **843**, 155973.
41 S. H. Wang, C. Fan, Z. Q. Zhao, Q. Liu, G. Xu, M. H. Wu, J. J. Chen and J. H. Li, *Appl. Catal., A*, 2020, **597**, 117554.
42 E. H. Gao, G. J. Sun, W. Zhang, M. T. Bernards, Y. He, H. Pan and Y. Shi, *Chem. Eng. J.*, 2020, **380**, 122397.
43 S. H. Li, B. C. Huang and C. L. Yu, *Catal. Commun.*, 2017, **98**, 47–51.
44 X. J. Yao, K. L. Ma, W. X. Zou, S. G. He, J. B. An, F. M. Yang and L. Dong, *Chin. J. Catal.*, 2017, **38**, 146–159.
45 X. J. Yao, T. T. Kong, S. H. Yu, L. L. Li, F. M. Yang and L. Dong, *Appl. Surf. Sci.*, 2017, **402**, 208–217.
46 Y. Peng, K. Z. Li and J. H. Li, *Appl. Catal., B*, 2013, **140–141**, 483–492.
47 F. Zhou, H. B. Song, H. Q. Wang, S. Komarneni and C. J. Yan, *Appl. Clay Sci.*, 2018, **166**, 9–17.
48 K. J. Lee, P. A. Kumar, M. S. Maqbool, K. N. Rao, K. H. Song and H. P. Ha, *Appl. Catal., B*, 2013, **142–143**, 705–717.
49 S. S. Liu, H. Wang, Y. Wei and R. D. Zhang, *Mol. Catal.*, 2020, **485**, 110822.
50 Y.-H. Lin, T.-C. Chiu, H.-T. Hsueh and H. Chu, *Appl. Surf. Sci.*, 2011, **258**, 1581–1586.
51 Q. Yu, R. Manfred, L. D. Li, F. X. Kong, G. J. Wu and N. J. Guan, *Catal. Commun.*, 2010, **11**, 955–959.
52 M. Romeo, K. Bak, J. E. Fallah, F. L. Normand and L. Hilaire, *Surf. Interface Anal.*, 1993, **20**, 508–512.
53 J. Cheng, L. Y. Song, R. Wu, S. N. Li, Y. M. Sun, H. T. Zhu, W. G. Qiu and H. He, *J. Rare Earths*, 2020, **38**, 59–69.
54 Q. L. Wang, J. J. Zhou, J. C. Zhang, H. Zhu, Y. H. Feng and J. Jin, *Aerosol Air Qual. Res.*, 2020, **20**, 477–488.
55 R. Sounak, B. Viswanath, M. S. Hegde and M. Giridhar, *J. Phys. Chem. C*, 2008, **112**, 6002–6012.
56 S. Ali, L. Q. Chen, Z. B. Li, T. R. Zhang, R. Li, S. H. Bakhtiar, X. S. Leng, F. L. Yuan, X. Y. Niu and Y. J. Zhu, *Appl. Catal., B*, 2018, **236**, 25–35.
57 S. Roy, B. Viswanath, M. S. Hegde and G. Madras, *J. Phys. Chem. C*, 2008, **112**, 6002–6012.
58 S. C. Li, W. J. Huang, H. M. Xu, T. J. Chen, Y. Ke, Z. Qu and N. Q. Yan, *Appl. Catal., B*, 2020, **270**, 118872.
59 H. D. Xu, Y. Wang, Y. Cao, Z. T. Fang, T. Lin, M. C. Gong and Y. Q. Chen, *Chem. Eng. J.*, 2014, **240**, 62–73.
60 H. Chitsazi, R. Wu, N. Q. Zhang, J. D. He, G. Z. Zhang and H. He, *Catal. Lett.*, 2020, **150**, 2688–2694.
61 X. X. Wang, Y. Shi, S. J. Li and W. Li, *Appl. Catal., B*, 2018, **220**, 234–250.
62 K. I. Hadjiivanov, *Catal. Rev.: Sci. Eng.*, 2000, **42**, 71–144.
63 X. J. Yao, R. D. Zhao, L. Chen, J. Du, C. Y. Tao, F. M. Yang and L. Dong, *Appl. Catal., B*, 2017, **208**, 82–93.
64 K. I. Hadjiivanov, *Catal. Rev.*, 2000, **42**, 71–144.
65 L. Chen, Z. Si, X. Wu and D. Weng, *ACS Appl. Mater. Interfaces*, 2014, **6**, 8134–8145.
66 E. H. Gao, B. Huang, Z. L. Zhao, H. Pan, W. Zhang, Y. N. Li, M. T. Bernards, Y. He and Y. Shi, *Catal. Sci. Technol.*, 2020, **10**, 4752–4765.
67 J. Yang, S. Ren, Y. H. Zhou, Z. H. Su, L. Yao, J. Cao, L. J. Jiang, G. Hu, M. Kong, J. Yang and Q. C. Liu, *Chem. Eng. J.*, 2020, **397**, 125446.